Achromatopsia—Visual Cortex Stability and Plasticity in the Absence of Functional Cones

Barbara Molz,[1,2,3] Anne Herbik,[2] Heidi A. Baseler,[1,4,5] Peter de Best,[6] Noa Raz,[6] Andre Gouws,[1,7] Khazar Ahmadi,[2] Rebecca Lowndes,[7] Rebecca J. McLean,[8] Irene Gottlob,[8] Susanne Kohl,[9] Lars Choritz,[2] John Maguire,[10,11] Martin Kanowski,[12] Barbara Käsmann-Kellner,[13] Ilse Wieland,[14] Eyal Banin,[15] Netta Levin,[6] Antony B. Morland,[1,5,7] and Michael B. Hoffmann[2,16]

[1]Department of Psychology, University of York, Heslington, York, United Kingdom
[2]Department of Ophthalmology, University Hospital, Otto-von-Guericke University, Magdeburg, Germany
[3]Language & Genetics Department, Max Planck Institute for Psycholinguistics, Nijmegen, the Netherlands
[4]Hull York Medical School, University of York, Heslington, York, United Kingdom
[5]York Biomedical Research Institute, University of York, Heslington, York, United Kingdom
[6]fMRI Unit, Department of Neurology, Hadassah Medical Center, Jerusalem, Israel
[7]York Neuroimaging Centre, Department of Psychology, University of York, York, United Kingdom
[8]University of Leicester Ulverscroft Eye Unit, University of Leicester, Leicester Royal Infirmary, Leicester, United Kingdom
[9]Molecular Genetics Laboratory, Institute for Ophthalmic Research, Centre for Ophthalmology, University Clinics Tübingen, Tübingen, Germany
[10]School of Optometry and Vision Sciences, University of Bradford, Bradford, United Kingdom
[11]Department of Neurophysiology, Children's Health Ireland (CHI) at Crumlin, Dublin, Ireland
[12]Department of Neurology, University Hospital, Otto-von-Guericke University, Magdeburg, Germany
[13]Department of Ophthalmology, Saarland University Hospital and Medical Faculty of the Saarland University Hospital, Homburg, Germany
[14]Department for Molecular Genetics, Institute for Human Genetics, University Hospital, Otto-von-Guericke University, Magdeburg, Germany
[15]Center for Retinal and Macular Degenerations, Department of Ophthalmology, Hadassah-Hebrew University Medical Center, Jerusalem, Israel
[16]Center for Behavioral Brain Sciences, Magdeburg, Germany

Correspondence: Michael B. Hoffmann, Department of Ophthalmology, University Hospital, Otto-von-Guericke University, Magdeburg 39120, Germany; michael.hoffmann@med.ovgu.de.

AH and HB as second authors and NL, AM, and MBH as senior authors contributed equally to this work.

BM, AH, HB, PB, NR, AG, KA, NL, AM, and MBH are NextGenVis consortium members.

Received: January 20, 2023
Accepted: August 7, 2023
Published: October 17, 2023

Citation: Molz B, Herbik A, Baseler HA, et al. Achromatopsia—visual cortex stability and plasticity in the absence of functional cones. *Invest Ophthalmol Vis Sci.* 2023;64(13):23. https://doi.org/10.1167/iovs.64.13.23

Purpose. Achromatopsia is a rare inherited disorder rendering retinal cone photoreceptors nonfunctional. As a consequence, the sizable foveal representation in the visual cortex is congenitally deprived of visual input, which prompts a fundamental question: is the cortical representation of the central visual field in patients with achromatopsia remapped to take up processing of paracentral inputs? Such remapping might interfere with gene therapeutic treatments aimed at restoring cone function.

Methods. We conducted a multicenter study to explore the nature and plasticity of vision in the absence of functional cones in a cohort of 17 individuals affected by autosomal recessive achromatopsia and confirmed biallelic disease-causing *CNGA3* or *CNGB3* mutations. Specifically, we tested the hypothesis of foveal remapping in human achromatopsia. For this purpose, we applied two independent functional magnetic resonance imaging (fMRI)–based mapping approaches, i.e. conventional phase-encoded eccentricity and population receptive field mapping, to separate data sets.

Results. Both fMRI approaches produced the same result in the group comparison of achromatopsia versus healthy controls: sizable remapping of the representation of the central visual field in the primary visual cortex was not apparent.

Conclusions. Remapping of the cortical representation of the central visual field is not a general feature in achromatopsia. It is concluded that plasticity of the human primary visual cortex is less pronounced than previously assumed. A pretherapeutic imaging workup is proposed to optimize interventions.

Keywords: achromatopsia, fMRI, plasticity, primary visual cortex, human

Gene-therapeutic interventions are of great promise to revolutionize medicine. Ophthalmologic diseases affecting retinal function take a pioneering role in this respect. This has been demonstrated for *RPE65*-related Leber congenital amaurosis before[1,2] and ultimately resulted in recent approval of voretigene neparvovec (Luxturna,

Spark Therapeutics, Inc., Philadelphia, USA), the first gene-therapeutic drug for an inherited retinal disease. Another disease that is currently a target of gene supplementation approaches is autosomal recessive achromatopsia (ACHM) (animal studies[3–8]; human trials: several human phase I/II trials are completed or in progress for ACHM related to *CNGA3* and *CNGB3* mutations: NCT03758404 and NCT03001310, Farahbakhsh et al.,[9] NCT02935517,[10] NCT02599922,[11] NCT02610582[12]). ACHM is a rare condition (1:30,000) with autosomal recessive inheritance and congenital dysfunction of the retinal cone photoreceptors[13–15] associated with reduced visual acuity, nystagmus, photophobia, and absent/severely impaired color vision.[16,17] Mutations in genes encoding functional components of the phototransduction cascade can cause ACHM. Mutations in two genes, *CNGA3* and *CNGB3*, account for >90% of the cases, while other genes (*GNAT2*, *PDE6C*, *PDE6H*, and *ATF6*) account for the remaining minority of cases.[18–20]

As the fovea is rod free, one far-reaching consequence of the congenital absence of cone function in ACHM is missing visual input to the foveal representation in the visual cortex. In the absence of plasticity, it would leave a large expanse of visual cortex deafferented. This prompts the question of whether the foveal representation is remapped to take up processing of input from more peripheral retina.[21–30] Such cortical reorganization might cause failure and undesired side effects of gene-therapeutic interventions. Therefore, the possibility of visual system plasticity has, beyond its relevance for our basic understanding of human visual cortex plasticity, direct clinical implications. For the visual cortex in ACHM, a pioneering case series study suggested substantial remapping of the foveal representation in the primary visual cortex,[31] and recently we described structural changes.[32,33] Such deviation from normal visual cortex structure and function might be a barrier to the success of upcoming novel therapeutic developments that aim to restore normal visual function in ACHM. Consequently, a systematic assessment of a larger cohort of genetically confirmed achromatic participants is important to determine whether remapping of the central visual field representation is a general feature of ACHM. We have therefore addressed this need with a multicenter functional magnetic resonance imaging (fMRI) study mapping the primary visual cortex (V1) in ACHM, with a sizable cohort of participants with confirmed biallelic disease-causing mutations in *CNGA3* or *CNGB3*. We specifically addressed the question of remapping of the foveal representation in ACHM with fMRI for both photopic and dark-adapted scotopic conditions.

Materials and Methods

Participants

A total of 17 individuals (Table 1) with genetically confirmed ACHM (10 *CNGA3* related and 7 *CNGB3* related) and absence of cone function confirmed with electroretinograms recorded according to ISCEV (International Society for Clinical Electrophysiology of Vision) standard[34] and 19 controls with no neurologic and ophthalmologic history and normal visual acuity were examined at three study sites: Hadassah Medical Center (HMC), University of Magdeburg (UM), and University of York (UY) (for comparability across sites, see "Cross-Site Comparability").

HMC: Six ACHM participants (mean ± SD age, 38.17 ± 5.64 years; four males) were referred for scanning by the Ophthalmology Department at HMC and three controls (mean ± SD age, 25.67 ± 7.02 years; two males) with normal or corrected-to-normal vision were recruited.

UM: Six ACHM participants (mean ± SD age, 25.00 ± 13.46 years; three males) and eight participants (mean ± SD age, 36.75 ± 11.99 years; four males) with normal or corrected-to-normal vision were recruited for scanning.

UY: Five ACHM participants (mean ± SD age, 40.17 ± 10.23 years; three males) were referred for scanning by collaborative sites. Eight controls (mean ± SD age, 26.23 ± 4.4 years; four males) with normal or corrected-to-normal vision were recruited from the York NeuroImaging Centre participant pool.

Each participant underwent up to two independent fMRI sessions, including a high-resolution structural scan. In each fMRI session, up to four functional population receptive fields (pRFs) and two phase-encoded runs were obtained. All participants provided informed consent to take part in the study. Experimental protocols received approval from the respective ethics committee and were in accordance with the Declaration of Helsinki. For ACHM, standard clinical history, including affected gene and rod function, was known, either through clinical tests carried out at the respective site or by the collaborators.

Data Acquisition

Imaging Parameters. UY: All scans were acquired using a 3T SIEMENS MAGNETOM Prisma scanner at the York Neuroimaging Centre (YNIC), UK. In brief, for high-resolution anatomic images, one T1-weighted scan (TR (Repetition time), 2500 ms; TE (Time to echo), 2.26 ms; TI (Inversion time), 900 ms; voxel size, 1 × 1 × 1 mm^3; flip angle, 7°; matrix size, 256 × 256 × 176) was acquired using a 64-channel head coil. All functional scans were acquired using a standard EPI sequence and the posterior part (40 channels) of the head coil (TR, 1500 ms; TE, 23 ms; voxel size, 2.5 × 2.5 × 2.5 mm^3; flip angle, 80°; matrix size, 64 × 64 × 30). The axial slices were aligned with the calcarine sulcus and placed to cover the whole occipital cortex. Additionally, for each fMRI session, a proton density scan with the same spatial prescription was acquired to facilitate alignment to the high-resolution structural scan.

HMC: All scans were acquired using a 3T SIEMENS MAGNETOM Skyra scanner at the Edmond & Lily Safra Center for Brain Sciences, Hebrew University of Jerusalem.

For high-resolution anatomical images, one T1-weighted scan (TR, 2300 ms; TE, 1.5 ms; TI, 900 ms; voxel size, 1 × 1 × 1 mm^3; flip angle, 9°; matrix size, 256 × 256 × 160), using a 32-channel head coil, was acquired. All functional scans were acquired using a standard EPI sequence and the posterior part of the head coil (TR, 1500 ms; TE, 27 ms; voxel size, 2.5 × 2.5 × 2.5 mm^3; flip angle, 70°; matrix size, 72 × 72 × 20). The coronal slices were aligned perpendicular to the calcarine sulcus and placed to cover the whole occipital cortex.

For each fMRI session, a T1-weighted FLASH inplane scan was acquired to facilitate alignment of functional scans to the high-resolution structural scan.

UM: All scans were acquired using a 3T SIEMENS MAGNETOM Prisma scanner at the University Hospital, Magdeburg. For high-resolution anatomic images, one T1-weighted scan (TR, 2500 ms; TE, 2.82 ms; TI, 1100 ms; voxel size, 1 × 1 × 1 mm^3; flip angle, 7°; matrix size, 256 × 256 × 192) was acquired using the posterior 40 channels of a 64-channel head coil. Similarly, for all functional scan sessions, only the posterior part of the coil was used, covering the

Table 1. Participant Demographics

Participant	Site	pRF	Luminance	TWA	Luminance	Age, y	Sex	Genotype	VA LogMAR
ACHM	HMC	3	S	2	S	34	M	*CNGA3*	0.7
ACHM	HMC	4	P/S	2	P/S	41	M	*CNGA3*	0.9
ACHM	HMC	3/4	P/S	2	P/S	35	M	*CNGA3*	1.0
ACHM (1)	HMC	4	P/S	1/2	P/S	41	F	*CNGA3*	0.7
ACHM (2)	HMC	4/2	P/S	2	P/S	42	F	*CNGA3*	0.8
ACHM	HMC	2	P/S	2	P/S	28	M	*CNGA3*	0.9
ACHM	UM	4/2	P/S	2	P	45	M	*CNGB3*	0.8
ACHM	UM	4/2	P/S	2	P	16	M	*CNGB3*	1.0
ACHM	UM	4/2	P/S	2/1	P/S	27	F	*CNGB3*	0.7
ACHM	UM	4/2	P/S	2	P	16	F	*CNGB3*	0.8
ACHM	UM	4	P	2	P	18	F	*CNGA3*	0.9
ACHM	UM	4/2	P/S	2	P	22	M	*CNGA3*	0.9
ACHM (3)	**UY**	4	P/S	2	P/S	40	F	*CNGB3*	1.5
ACHM	UY	4	P	2	P	28	M	*CNGB3*	1.9
ACHM	UY	2/4	P/S	1/2	P/S	34	M	*CNGB3*	1.9
ACHM	UY	4	P/S	2	P/S	34	M	*CNGA3*	0.8
ACHM	UY	4	S	2	S	51	F	*CNGA3*	1.0
HC	HMC	2/3	P/S	2	P/S	25	M		
HC	HMC	4	P/S	2	P/S	33	F		
HC	HMC	4	P/S	2	P/S	19	M		
HC	UM	4	P/S	2	P/S	27	M		
HC	UM	4	P/S	/	/	33	M		
HC	UM	4	P/S	2	P/S	58	F		
HC	UM	4	P/S	2	P/S	29	M		
HC	UM	4	P/S	2	P/S	53	F		
HC	UM	4	P	2	P	27	M		
HC	UM	4	P	2	P	35	F		
HC	UM	4	P	2	P	32	F		
HC	UY	4	P/S	2	P/S	25	F		
HC	UY	4	P/S	2	P/S	25	F		
HC	UY	4	P/S	2	P/S	34	M		
HC	UY	4	P/S	2	P/S	28	M		
HC	UY	4	P/S	2	P/S	24	M		
HC	UY	4	P/S	2	P/S	20	F		
HC	UY	4	P/S	2	P/S	30	F		
HC	UY	4	P/S	2	P/S	23	M		

Summary of participant groups, scanner site, age and sex, and acquired number of pRF or phase-encoded analysis (TWA) stimulus runs for each luminance condition. If just one number is denoted for either pRF or phase-encoded runs, this number is representative for all indicated luminance levels. Participants marked in bold match participants later referred to in the article. P, photopic; S, scotopic; TWA, traveling wave analysis.

region of the occipital cortex using a multiband-accelerated (factor 2) EPI sequence (TR, 1500 ms; TE, 30 ms; voxel size, 2.5 × 2.5 × 2.5 mm^3; flip angle, 80°; matrix size, 84 × 84 × 54). The axial slices were aligned with the calcarine sulcus and placed to cover the whole occipital cortex.

Visual Stimuli

All stimuli were generated using the Psychophysics Toolbox Version 3[35–37] in conjunction with 32-bit MATLAB (Version 7.6.0; The MathWorks, Natick, MA, USA). For both phase-encoded eccentricity mapping[38–40] and pRF mapping,[41] a modified, nonscaled version of the previously described stimuli was used (Fig. 1). Briefly, an unmasked portion of a 100% contrast flickering checkerboard (width 2°) was presented on a mean gray background (equivalent to the average luminance of the checkerboard) within a circular aperture (8° radius). Spatial (fundamental = 0.25 cycle/°) and temporal frequencies (2-Hz square wave contrast reversal) were adjusted for both stimuli to maximize responses under low luminance levels.

For all phase-encoded retinotopy runs, the ring stimulus increased from the center of the visual field and was replaced by a new central annulus during the last step of each cycle. Each stimulus run lasted 48 seconds and was repeated for seven full cycles. For pRF, mapping the bar stimulus was swept in one of eight different directions within a circular aperture. Each sweep lasted a total of 48 seconds and included four blank gray mean luminance periods (12 seconds each) as baseline conditions at the end of sweeps 1, 3, 5, and 7.

Participants were instructed to maintain central fixation at the perceived intersection of a large diagonal X, which alternated every 2 seconds between black and white to minimize a potential Troxler effect.[42] To avoid any interference with central visual field regions, the fixation cross included a central gap of 2° diameter. Participants completed an attention task and were instructed to respond with a button press every time the fixation cross doubled in width. Changes in width occurred randomly, no more than once within 12 seconds but at least every 36 seconds. Reaction time and percentage correct for the attention task were recorded for each functional run.

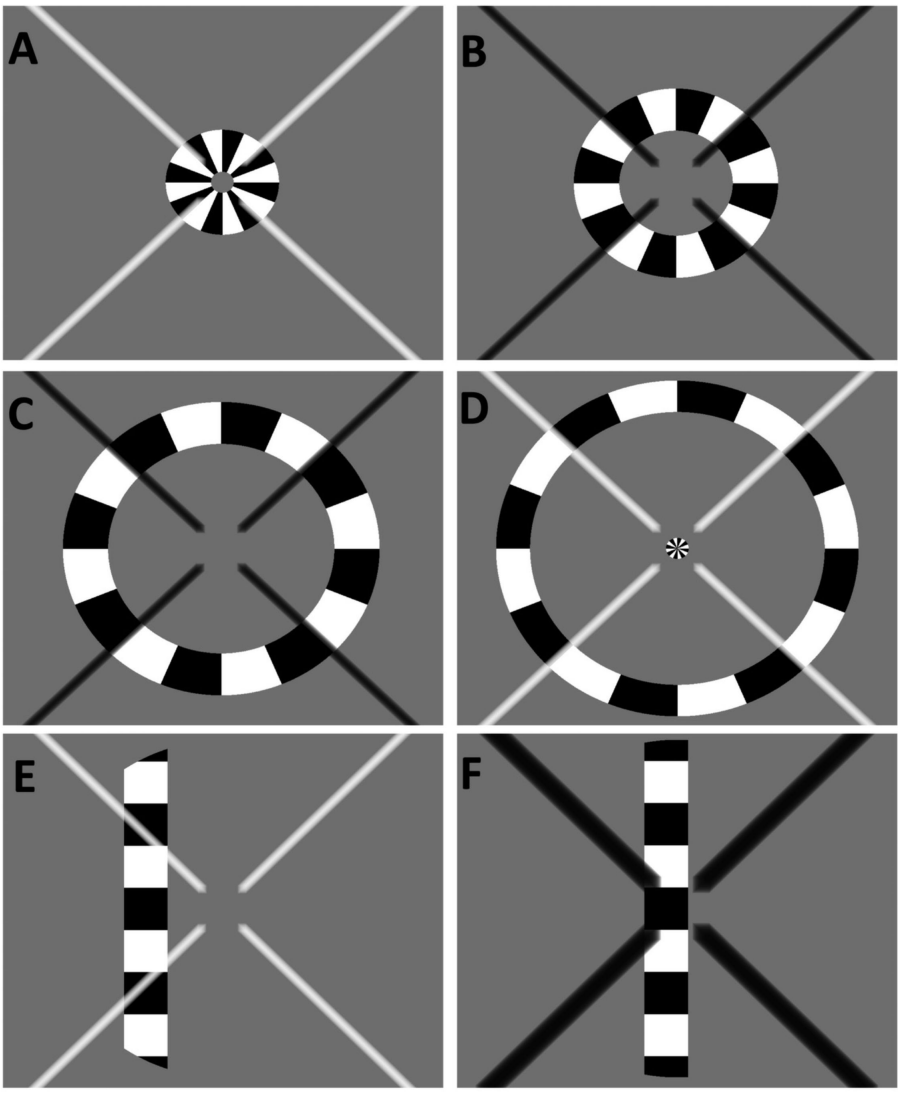

Figure 1. Example of the visual stimuli used for retinotopic mapping. (**A–D**) A sample of the contrast-reversing ring stimuli used for phase-encoded eccentricity mapping that illustrate a few sample steps of a single stimulus cycle. Note that in (**D**), the stimulus starts again in the center of the visual field, while the previous cycle is still in its final stage, commonly referred to as "wraparound." (**E**, **F**) The stimuli used for pRF mapping. (**E**) General stimulus features. In all panels, the *fixation cross* is overlaid and includes a central gap. In (**F**), the *fixation cross* has the target size for the attention task (doubled width).

Stimulation software was shared across sites to ensure identical stimulus presentation despite different presentation hardware:

UY: Stimuli were rear-projected onto an acrylic screen situated in the bore of the scanner behind the participant's head using an LCD projector (PROPixx DLP LED Projector; VPixx Technologies, Canada). All participants viewed the screen via a mirror mounted on the head coil at a viewing distance of 57 cm.
HMC: Stimuli were presented on a 32-in. MR-compatible LCD monitor (NordicNeuroLab, Bergen, Norway) situated at the end of the scanner bore behind the participants' head. All participants viewed the screen via a mirror mounted on the head coil at a viewing distance of 131 cm.
UM: Stimuli were rear-projected onto an acrylic screen situated in the bore of the scanner behind the participants' head using a D-ILA Projector (JVC, Bad Vilbel, Germany; DLA-RS49). All participants viewed the screen via a mirror mounted on the head coil at a viewing distance of 35 cm.

In general, two different luminance settings were used: a bright-light condition, referred to as "photopic," and a low-luminance condition, referred to as "scotopic." For two scanner sites, a second photopic condition with reduced light was added for scanning achromats (Table 2).

For low-photopic conditions in UY and UM (mean luminance: 10 and 7 cd/m^2, respectively), a neutral density filter (Formatt Hitech, UK; Firecrest ND 85 × 85 mm, ND 1.5) was mounted in front of the projector to reduce the overall luminance. For the scotopic condition, all participants wore customized goggles fitted with layers of neutral density foils (Stage Depot Limited, UK; Neutral Density Rosco E-Colour+ lighting filter sheet) to achieve the specified luminance.

Table 2. Overview of Mean Luminance Settings Used at the Participating Scanner Sites

Site	Photopic, cd/m^2		Scotopic, cd/m^2
	Control	Patient	All Participants
UY	300	10	0.05
UM	220	7	0.05
HMC	200		0.05

UY and UM used two different photopic settings depending on the participant group while the setup at HMC only allowed for one photopic setting. Scotopic luminance levels were identical across sites.

During scanning, all light sources in the scanner rooms were switched off. For all scotopic scans, participants were dark-adapted for a minimum of 30 minutes prior to data acquisition. For all scans, participants viewed the presented stimuli monocularly, whereby a patch occluded the nondominant eye. To establish eye dominance, the Porta Test (point-a-finger test)[43–45] was used. All participants were instructed to extend an arm and align a finger with a distant corner. The participants were then instructed to alternately close one eye and report which eye was aligned with the target, which was then noted as the dominant eye.

The influence of differences in luminance settings across sites is separately addressed in a site comparison (see Methods, Results, and Limitation section in the Discussion).

Data Preprocessing

UY: High-resolution T1-weighted scans were automatically segmented into gray and white matter using the Freesurfer analysis suite 5.3[46,47] (http://surfer.nmr.mgh.harvard.edu/). The output was manually corrected for potential segmentation errors (ITK_Snap,[48] www.itksnap.org) and the cortical surface reconstructed to create an inflated three-dimensional (3D) mesh, used for visualization of derived retinotopic maps and ROI (Region of Interest) definition. Proton density scans were FAST corrected using the FSL toolbox (https://www.fmrib.ox.ac.uk/fsl, FSL[49]) and skull stripped BET (Brain Extraction Tool), to facilitate alignment with the high-resolution structural scan. Functional data were preprocessed and analyzed mainly with the mrVista toolbox (VISTASOFT software package, https://www.stanford.edu/group/vista/cgi-bin/home/software) run on MATLAB 8.0 (2012b). In brief, dummy volumes (8) were discarded and data were motion corrected.

HMC: Preprocessing of anatomic data was identical to the UY workflow. The functional analysis stream was adapted and initial steps were carried out in FSL. In brief, dummy volumes (8) were discarded, and within-scan motion correction was carried out with FSL's MC FLIRT final (internal) sinc interpolation.[50] After this stage, all functional scans were aligned to the first used functional volume, similar to the mrVista approach, using FSL's FLIRT.

UM: T1-weighted anatomic scans were automatically segmented using FreeSurfer (5.3) (http://surfer.nmr.mgh.harvard.edu/)[46,47] and the cortical surface reconstructed to create an inflated 3D mesh, used for visualization of derived retinotopic maps and ROI definition. Functional preprocessing was first carried out using the FSL toolbox (https://www.fmrib.ox.ac.uk/fsl) for motion correction.

For all sites, corrected runs with large motion artifacts or poor performance on the attention task were excluded. The exclusion of runs was mostly based on large fluctuations of the time series, as typical for large motion artifacts. As the same analyst conducted the data processing, no systematic differences were noted and motion outliers could be seen across all sites and were generally sparse and not more remarkable than in other studies (see Table 1 for an overview of runs per participant). Remaining pRF or phase-encoded runs were averaged and aligned to the high-resolution T1-weighted images. This was done either using FSL (FLIRT) and mrVista tools (rxAlign,VISTASOFT software package) for data collected at UY and HCM or by using mrVista tools assisted by Kendrick Kay's alignment toolbox (github.com/kendrickkay/alignvolumedata) for data collected at UM.

Data Analysis

Cross-Site Comparability. To estimate the comparability of the acquired signal at each site, coherence values for both regions of interest and both luminance levels were extracted from the phase-encoded data set and plotted for each scanner site (after arcsine transformation to evaluate this statistically). Coherence values were used as they are calculated on the processed data (motion corrected, dummy volumes removed, averaged) and allow for a direct comparison of signal change as used in the subsequent analysis stream. A mixed model REML (Restricted Maximum Likelihood) as implemented in Prism 9.0 with ROI and luminance level as within-subject factors and site as a between-subject factor was applied and revealed, as expected, a main effect of luminance level ($F_{1, 32} = 23.37$; $P < 0.0001$) and ROI ($F_{1, 32} = 11.08$; $P = 0.0022$). Importantly, however, a main effect of scanner site ($F_{2, 32} = 0.2723$; $P = 0.7634$) and/or significant interaction terms were not found. As a consequence, the derived phase-encoded and pRF estimates were pooled across scanner sites for all reported analysis streams (Supplementary Fig. S1, Supplementary Table S1).

Processing of phase-encoded and pRF data. To determine the phase and therefore the eccentricity producing the maximum response for each voxel, the averaged phase-encoded eccentricity mapping runs were analyzed with the mrVista toolbox (VISTASOFT software package, https://www.stanford.edu/group/vista/cgi-bin/home/software), analogous to Kaule et al.,[51] which involved applying a Fourier analysis to the fMRI time series to obtain the amplitude and phase for each frequency and the calculation with a sinusoid with a frequency equal to that of the visual stimulation (1/48 Hz). Coherence (C) is defined as the Fourier amplitude of the blood oxygen level-dependent (BOLD) signal at the stimulus fundamental frequency divided by the sum of amplitudes of frequency bins around the fundamental.[52] The averaged pRF runs were used to determine both the eccentricity and polar angle information as well as pRF size. To determine the pRF-center position (x0, y0) and pRF size of each voxel, we used the previously described pRF-modeling approach implemented in the mrVista toolbox.[41]

Delineation of visual field maps. The analysis of the visual field maps made use of an anatomic retinotopy atlas[53,54] (implemented in the python analysis toolbox "neuropythy"). This atlas was used to create two ROI masks (FSL toolbox) for each participant, representing the central (0°–4°) and paracentral portions (4°–8°) of V1. For each participant, these two ROIs were imported to mrVista and manu-

ally traced on the participant's specific 3D mesh. Here, it should be noted that equal eccentricity bands of the ROIs do not result in equal-sized ROIs. Instead, due to cortical magnification, the resulting central ROI exceeds the paracentral ROI in size. On the other hand, it is well known that there are often dropouts of responses in the central cortical representation, particularly for scotopic stimulation. Consequently, equating SNRs (signal-to-noise-ratios) across ROIs and luminance conditions is not possible, and other strategies would likely introduce other biases. As a consequence, we chose equal widths for the two eccentricities. Importantly, a larger central ROI will tend to increase SNR for central responses and thus increase the sensitivity to the sign of remapping addressed in the present study (i.e., activations of the central visual field representation in ACHM).

A customized script was applied to identify and remove any voxels shared between the ROIs.[55] In addition, mean percent signal change values for each ROI were averaged across left and right hemispheres for all subsequent analyses.

Statistical Analysis

Phase-Encoded Analysis. *Single-cycle heatmaps.* Time-series data were extracted for each ROI (V1 central and paracentral) from the phase-encoded ring data set. The mean time series for each ROI and participant was inspected for potential artifacts. If spikes occurred simultaneously in both ROIs, an artifact was assumed and the affected cycle deleted. Time series were then averaged across cycles to generate a single-cycle average for each participant, ROI, and luminance level.

For each participant group, all single-cycle averages (percent signal change) were plotted as a heatmap for each luminance level and ROI. Individual modulations were averaged across the group and overlaid in red on each heatmap to show the overall luminance-specific time-series change within each ROI.

Population Receptive Field Mapping. Here, the proportion of early visual cortex that responded above threshold per luminance level was identified, and the number of voxels that exceeded 10% variance explained[56] in each pRF model fit was determined per participant for each ROI and divided by the total ROI voxel count. Subsequently, the mean eccentricity and mean pRF size of voxels that exceeded 10% variance in each pRF model fit were calculated for each participant, per condition and ROI.

For all three described pRF analysis measures, two-way ANOVAs were applied on the dependent variables "amplitude" (for phase-encoded eccentricity mapping) and "percentage active voxels," "mean eccentricity," and "mean pRF size" (for pRF mapping) to determine the main effect of ROI and participant GROUP and the interaction between these two factors (GROUP × ROI) at each luminance level. For potential post hoc comparisons, an independent sample *t*-test was applied for each ROI to test for an effect of the participant group on "percentage active voxels," "mean eccentricity," and "mean pRF size."

Graphs (line graphs, box-and-whisker plots) were created using Prism version 8.00 for Mac (GraphPad Software, La Jolla, CA, USA) while all other graphs were created using MATLAB (2017a).

Results

Below, the results are given for (1) the phase-encoded eccentricity mapping and (2) different outcome measures of the pRF-based mapping. Given the multicenter nature of this study, we first tested the comparability of our data across the different sites and found no effect of scanner site (see Methods, Supplementary Fig. S1, Supplementary Table S1). Consequently, the data for all subsequent analysis streams were combined.

Phase-Encoded Eccentricity Mapping of Primary Visual Cortex (V1)

Baseler et al.[31] suggested V1 remapping in ACHM, based on a case series employing phase-encoded fMRI. We revisited this issue in a larger participant sample. We began with an assessment that resembles this initial study. For better comparability with Baseler et al.,[31] we therefore first applied conventional phase-encoded eccentricity mapping based on the stimulation with expanding rings for both photopic and scotopic conditions. A qualitative overview of the obtained maps is presented in Figure 2 depicting the visual cortex of the left hemispheres of a healthy control (HC) and three representative ACHM participants spanning a range of visual acuities (0.7–1.5 logMAR) that were selected to demonstrate the range of cortical responses observed. Orderly eccentricity maps were obtained in the control and in two of the three ACHM participants depicted (ACHM1/2). In contrast, for the ACHM participant with low visual acuity (ACHM3), hardly any cortical responses were evident irrespective of the luminance condition. For scotopic stimulation, in both the control and the participants ACHM1/2, the peripheral and parafoveal visual field representations of V1 were largely similar to those for photopic stimulation. In contrast, the cortical region in V1 that represents the more central retina, including the rod-free foveal zone, lacks, in both the control and ACHM1/2, the BOLD signals that were evident during photopic stimulation. The patterns shown in Figure 2 are broadly representative of the group data. This is taken as evidence for the absence of remapping of V1 in ACHM, as further supported by the quantitative analyses given in the supplementary material (Supplementary Fig. S2).

Population Receptive Field Mapping

While we assessed central visual responses in ACHM with conventional eccentricity mapping analogous to Baseler et al.,[31] our main focus was to applied the more contemporary pRF mapping to examine responses in ACHM in more detail, where we compared responses in atlas-based definitions of $ROI_{central}$ and $ROI_{paracentral}$. The three measures taken to assess responses within central representations of V1 were (1) the proportion of the respective V1 ROI that was responsive (measured in percentages), (2) the mean visual field eccentricity of the responses in the ROIs, and (3) the mean pRF size of responses in each V1 ROI. They test the hypothesis that foveal remapping in ACHM would specifically affect the central visual representation ($ROI_{central}$) but not the paracentral representation ($ROI_{paracentral}$) in ACHM in the different fMRI measures: pRF-based V1 coverage would increase, pRF-eccentricity would increase, and pRF size would decrease relative to HCs. To address this, two-way mixed ANOVAs were applied separately for each luminance condition (factors GROUP (HC/ACHM) and ROI ($ROI_{central}$/$ROI_{paracentral}$)) and a response signature that indi-

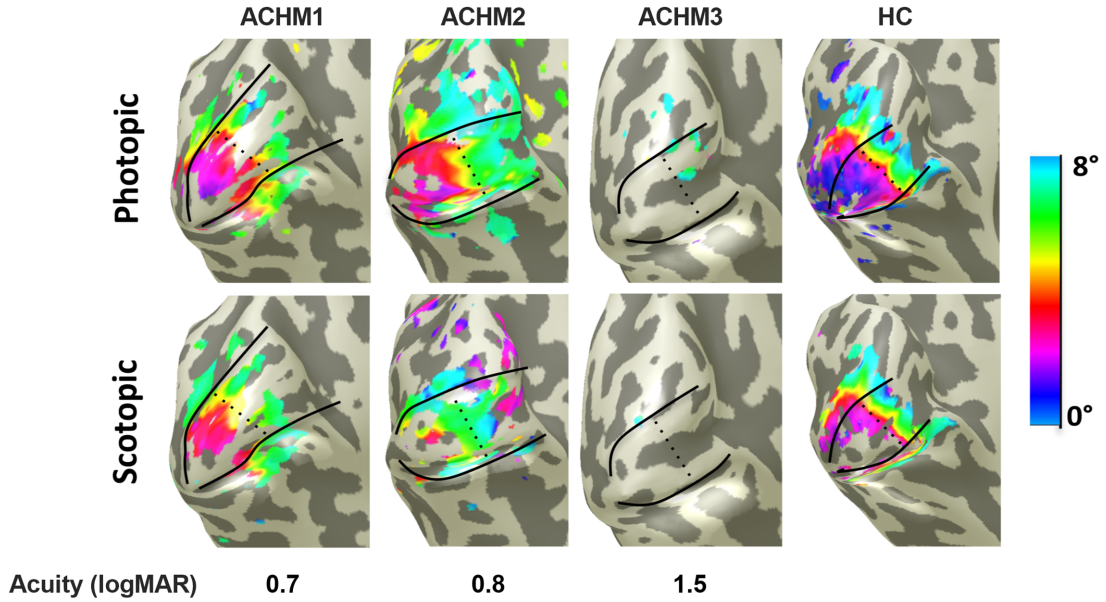

Figure 2. Eccentricity representations in V1 under different luminance levels derived from conventional phase-encoded eccentricity mapping for three representative participants with achromatopsia (ACHM) and a healthy control participant (HC). All maps are projected onto the left hemisphere of an inflated 3D mesh of the occipital lobe; the boundaries of V1, with atlas-based subdivisions of central and paracentral representations, are outlined in *black*. Data were thresholded at a coherence value ≥0.25, corresponding to $P < 0.0001$.[57]

cates remapping would be reflected by a significant interaction of GROUP × ROI in the mixed-luminance comparison, as detailed in supplementary material ("Rationale—ROI Selection and Relevance of the Interaction GROUP × ROI").

Proportion of Cortex Responding to Visual Stimulation. For both photopic (Fig. 3A) and scotopic stimulation (Fig. 3B), patients with ACHM exhibited a lower proportion of overall activated V1 than HCs. This effect appears independent of ROI and is supported by the ANOVAs conducted that showed significant main effects, but no significant interaction of GROUP × ROI (photopic: GROUP: $F_{1, 31} = 24.99$, $P = 0.0001$; ROI: $F_{1, 31} = 6.867$, $P = 0.0135$; GROUP × ROI: $F_{1, 31} = 2.138$, $P = 0.1537$; scotopic: GROUP: $F_{1, 28} = 4.663$, $P = 0.0395$; ROI: $F_{1, 28} = 22.43$, $P = 0.0001$; GROUP × ROI: $F_{1, 28} = 0.45$, $P = 0.8338$). As pointed out in Methods ("Relevance of Mixed-Luminance Comparison"), the critical comparison to assess remapping in ACHM is the mixed-luminance comparison (Fig. 3C). A two-way mixed ANOVA only revealed an effect of ROI ($F_{1, 28} = 18.22$, $P = 0.0002$) but neither a main effect of GROUP ($F_{1, 28} = 0.0044$, $P = 0.8351$) nor an interaction of GROUP × ROI ($F_{1, 28} = .1178$, $P = 0.7340$). This absence of the interaction of GROUP × ROI for the mixed-luminance comparison indicates the absence of central V1 remapping in ACHM as a group. Finally, we observed a large range of visual acuities in ACHM (0.69–1.85 logMAR), measured under photopic conditions (Table 1). To investigate whether this might explain the large range of values for proportion of activated V1 in ACHM under photopic conditions (Fig. 3A), we tested the correlation between visual acuity and the proportion of activated V1, both under photopic conditions, and report significant correlations for both $ROI_{paracentral}$ ($P = 0.0016$) and $ROI_{central}$ ($P = 0.0409$), that is, the proportion of V1 active is higher for better visual acuity (i.e., reduced logMAR) in ACHM. This indicates that the proportion of V1 active might be a determinant of visual acuity in ACHM or vice versa.

Eccentricity Representations in V1. If remapping (i.e., the representation of the paracentral visual field in $ROI_{central}$) is present in ACHM individuals, this should result in representations of greater eccentricity values in $ROI_{central}$ in ACHM compared to HC (i.e., in a significant interaction of GROUP × ROI for the mixed luminance comparison) (see Rationale, Supplements). We analyzed the eccentricity values of the responses above threshold (>10% variance explained). For the photopic condition (Fig. 3D), greater eccentricity values were obtained in ACHM than for the controls. The ANOVA revealed significant main effects of GROUP ($F_{1, 31} = 17.43$, $P = 0.0002$) and ROI ($F_{1, 31} = 116.9$, $P < 0.0001$) and a significant interaction of GROUP × ROI ($F_{1, 31} = 8.889$, $P = 0.0055$). These effects are a consequence of the HC responses in the central representation being driven by cone signals, which are absent in ACHM. For the scotopic condition, as depicted in Figure 3E, the ANOVA did not reveal a main effect of GROUP ($F_{1, 28} = 1.807$, $P = 0.1897$) but a main effect of ROI ($F_{1, 28} = 55.54$, $P < 0.0001$) and a significant interaction of GROUP × ROI ($F_{1, 28} = 16.69$, $P = 0.0003$). At face value, these effects might appear to be driven by the ACHM group registering larger eccentricity in $ROI_{central}$. However, this must be cautioned against as the proportion of $ROI_{central}$ that exhibits responses that contribute to the pRF eccentricity estimate is very small for many members of the ACHM compared to HC group, as is evident from Figure 3B. The pRF eccentricity estimates may therefore be artifactually inflated as a result of a regression-to-the-mean effect in ACHM, as pointed out in supplementary material ("Rationale—Relevance of Mixed-Luminance Comparison," Supplements). In fact, there is a significant inverse correlation of eccentricity estimate versus proportion of V1 active ($F_{1, 13} = 6.07$, $P = 0.0285$), that is, an increase of eccentricity with a decrease of V1 active. Consequently, the critical comparison to assess remapping in ACHM is the mixed-luminance comparison (Fig. 3F) for which the proportion of responses exceeding our 10% threshold in the ROIs of

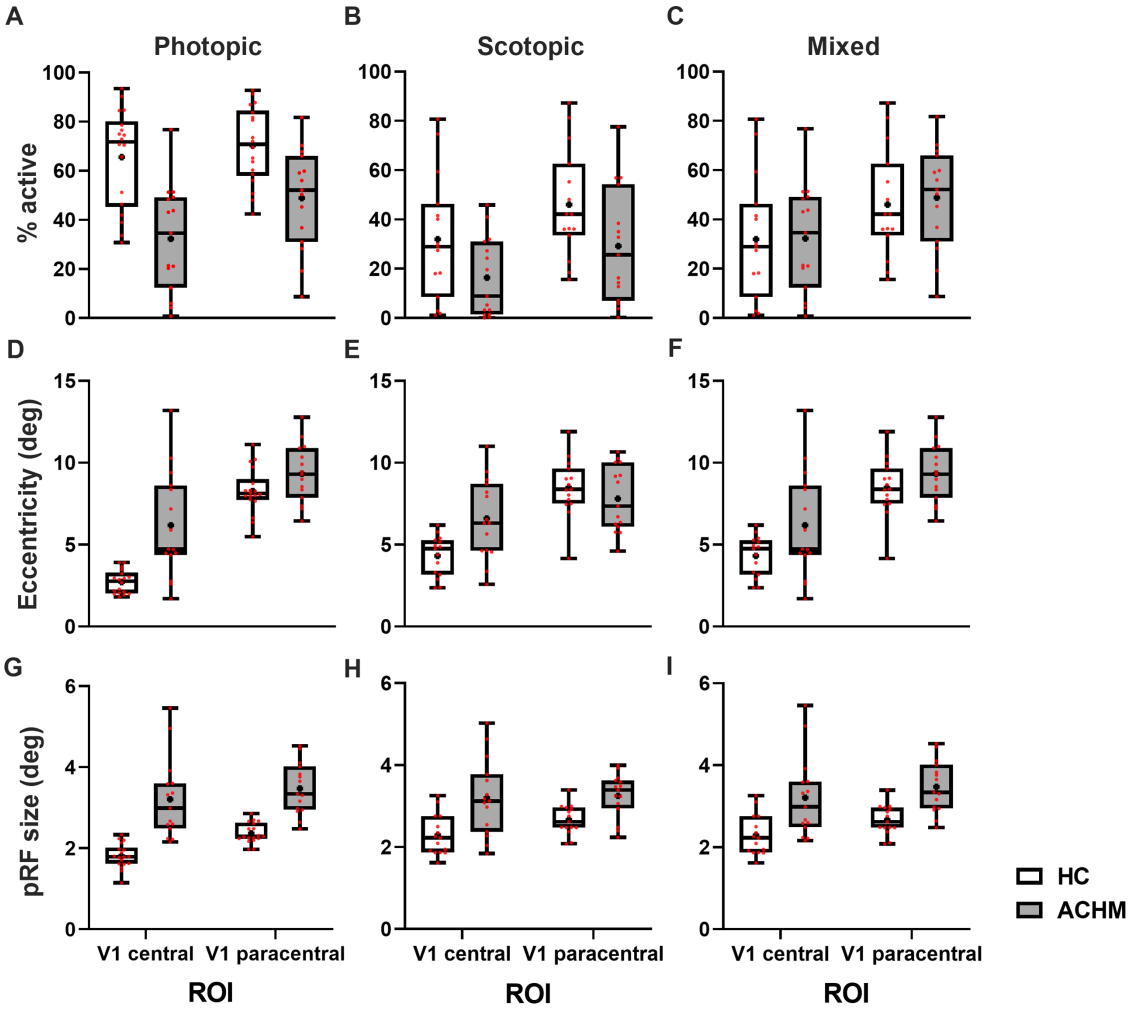

Figure 3. Population receptive field estimates in central and paracentral portions of V1 in HC and ACHM participants. *Top row*: Percentage of active voxels: (**A**) depicts visual cortical estimates derived under photopic conditions while (**B**) represents the percentage of V1 responding under scotopic conditions. In (**C**), luminance conditions are mixed and the percentage of V1 responding of controls under scotopic conditions is contrasted with the percentage of V1 responding within the respective ROI of ACHM derived under photopic conditions. *Middle row*: Mean eccentricity (in degrees) of $ROI_{central}$ and $ROI_{paracentral}$ in V1 shown for both participant cohorts under photopic (**D**), scotopic (**E**), and mixed (**F**) luminance conditions. *Bottom row*: Mean pRF size (in degrees) $ROI_{central}$ and $ROI_{paracentral}$ in V1 shown for both participant cohorts under photopic (**G**), scotopic (**H**), and mixed (**I**) luminance conditions. See text for details and statistics. *Whiskers* present minimum and maximum values, while the *box* extends from the 25th to 75th percentiles. Median and mean are shown by a *solid line* and a +, respectively; individual data points are shown in *red*; sample sizes: N_{HC} (photopic/scotopic) = 18/16; N_{ACHM} (photopic/scotopic) = 15/15.

each group is largely matched, as shown in Figure 3C. Here the ANOVA revealed a main effect of GROUP ($F_{1, 28} = 4.719$, $P = 0.038$) and ROI ($F_{1, 28} = 61.77$, $P < 0.001$), while an interaction of GROUP × ROI was not evident ($F_{1, 28} = 1.189$, $P = 0.285$). It should be noted that, in line with the assumption that less reliable data (with a low number of stimulus driven voxels) is linked with larger eccentricities, the similarity between ACHM and HC data in the mixed condition increases if participants with ≤20% active voxels are excluded from the analysis, highlighted by no main effect of GROUP (mixed model, $F_{1, 24} = 1.324$, $P = 0.2613$) and only a main effect of ROI ($F_{1, 18} = 121.6$, $P < 0.0001$) (Supplementary Fig. S3).

pRF Size of Responses in V1. Applying pRF mapping also allowed us to test pRF size differences between the cohorts. Reorganization might offer benefits in terms of increased spatial resolution, if initially enlarged and shifted pRFs reduce in size when reorganization is complete.[21] We tested for such effects on mean pRF sizes obtained for the two ROIs and groups. For the photopic condition, the mean pRF size was generally larger in $ROI_{paracentral}$ compared to $ROI_{central}$. ACHM exhibited overall larger pRF sizes than HC in both ROIs (Fig. 3G). An ANOVA revealed main effects of GROUP ($F_{1, 31} = 42.56$, $P < 0.0001$) and ROI ($F_{1, 31} = 27.09$, $P < 0.0001$), while an interaction of GROUP × ROI was not evident ($F_{1, 31} = 3.595$, $P = 0.0710$). Similarly, for the scotopic condition (Fig. 3H), differences in pRF size between ACHM and HC were also present, although less pronounced (GROUP: $F_{1, 28} = 16.61$, $P = 0.0003$). Again, the mean pRF size was generally larger in $ROI_{paracentral}$ compared to $ROI_{central}$, while the difference did not result in a main effect of ROI ($F_{1, 28} = 2.621$, $P = 0.1167$). No interaction of GROUP × ROI was evident ($F_{1, 28} = 1.473$, $P = 0.2351$). In line with the preceding results, larger population receptive fields were also found in ACHM compared to HC when comparing data for mixed-luminance comparison

(Fig. 3J). Again, while main effects of GROUP ($F_{1, 28} = 15.60$, $P = 0.0005$) and ROI ($F_{1, 28} = 9.603$, $P = 0.0044$) were observed, no interaction of GROUP × ROI was significant ($F_{1, 28} = 0.2806$, $P = 0.6005$). It appears, therefore, that instead of a refinement of pRFs to smaller sizes, ACHM leads to an increase in population receptive field size for both $ROI_{central}$ and $ROI_{paracentral}$. This independence of the effects from ROI shifts potential explanations of the observed effect away from plasticity of the central visual field representation, as generally enlarged receptive fields can come from multiple sources, including neural origin, eye movements, and potentially noise. In fact, nystagmus in the patients is a potential cause of increased pRF measures, while it leaves other pRF estimates relatively unaffected.[31,58–62]

Discussion

We explored the nature and plasticity of vision in the absence of functional cones applying fMRI assessments to ACHM associated with confirmed biallelic *CNGA3* and *CNGB3* mutations and electroretinographically confirmed absence of cone function. Two separate mapping approaches, conventional phase-encoded eccentricity and pRF mapping applied to independent data sets, produced the same result in terms of plasticity: sizable remapping of the representation of the central visual field in the primary visual cortex does not appear to be a general feature in ACHM.

Visual Cortex Organization in ACHM

Reorganization of the human visual cortex in response to abnormal input is topical and highly important for basic science and clinical applications. Generally, it is assumed that the plastic potential is higher for congenital than for acquired visual pathway defects,[24,25,52] and even for the former, sizable remapping at the level of the primary visual cortex appears to be limited.[23] For example, in congenital malformation of the optic chiasm, remapping of the cortical visual field representations does not appear to have the scope to compensate for lower-level abnormalities, but instead, adaptive mechanisms are confined to the microcircuitry of the primary visual cortex and to higher processing levels.[23,60,63,64] In the context of congenital visual system abnormalities, ACHM was viewed as a stronger example of macroscopic remapping. Here the deafferented representation of the central visual field in V1 appeared to be remapped to serve processing of paracentral visual field portions. This view was based on a previous case series study.[31] It is revisited in the present study with a group-based analysis with a comprehensive set of conventional and pRF mapping data that underwent independent analyses. It emerged that this scope of remapping of the representation of the central visual in V1 is not a group feature and might therefore be reserved to specific individuals with ACHM.[31] This conclusion is based on the comparison of V1 activation (amplitude and area) and pRF characteristics (eccentricity and size) between central and paracentral visual field representations in V1 of HC and ACHM. For better continuity to the preceding study,[31] a mixed-luminance comparison (scotopic HC versus photopic ACHM) was applied and no significant specific effects at the group level were evident. We explicitly aimed to maximize technical similarity between the 2002 study and our present one. However, not all conditions could be equalized (e.g., magnetic field strength, analysis pipeline), but these technical differences in the MRI approach are not a compelling cause of the different results. In fact, the 2003 abnormal visual cortex mapping in albinism has been reproduced many times since.[51,64,65] There is a more obvious difference between the two studies (i.e., the selection of study participants): the present study strictly excluded ACHM individuals with residual cone responses. In contrast, Baseler et al.[31] explicitly stated that two out of the three participants, including the one with the most prominent effects, did have residual cone function. Given the absence of V1 remapping in our group of 17 ACHM patients selected for the absence of cone responses, the critical feature of residual cone function in the previous study now appears a potential cause of the discrepancy in study outcomes.

Relation to Visual Cortex Structure in ACHM

How does the lack of functional plasticity in ACHM-V1 correspond to previous structural findings in ACHM? In our previous studies on visual cortex structure in ACHM, we observed changes, that is, V1 gray matter thickening for the central representation[32] and a generalized reduction of surface area in V1, V2, and V3.[33] These features in ACHM resemble cortical alterations that were previously reported for the visual cortex of congenitally blind individuals, where they were taken as an indicator of the lack of maturation of the cortex for visual processing, including changes of the myelination of the primary visual cortex.[66–75] In analogy, the previously reported structural changes of the visual cortex in ACHM might indicate a lack of maturation of a visual cortex that is deprived of cone input. As a consequence of this lack of maturation in ACHM, plastic mechanisms supporting the foveal remapping in V1 would be unexpected, which is in accordance with the functional characteristics of the visual cortex in ACHM described in the present fMRI study.

Relevance of Visual Cortex Mapping and Functioning in ACHM for Clinical Applications

The findings of the present study inform and support an individualized approach to medical care in ACHM. Specifically, they are important for developing treatments as well as for obtaining a comprehensive diagnostic picture of the affected individuals. This is particularly topical in the face of current ongoing clinical trials to establish gene therapies that aim at restoring cone function in ACHM (NCT03758404 and NCT03001310,[9] NCT02935517,[10] NCT02599922, NCT02610582).[11,12] One consequence of such therapies is the restoration of visual input to the deafferented central visual field representation in V1. If this representation has undergone remapping[31] prior to therapy, restoration of visual input might cause unexpected side effects (e.g., sensory conflicts), potentially counteracting the success of gene therapy. Similar to the results in the current large cohort study, the two patients with ACHM who were recently reported[10] exhibited large pRF sizes along the early visual cortex. Following gene augmentation therapy, their pRF sizes were reduced, suggesting that the visual cortex is able to respond to the new input.

In our group study, we now report that such reorganization is not a general feature of ACHM, at least in those without evidence of residual cone function. While this might

be taken as an indication that restoring cone input will not induce sensory conflicts in general, caution should be taken as remapping may be present in some individuals, such as those reported in Baseler et al.[31] Consequently, V1 mapping could form an important component of an individualized pretherapeutic clinical workup in ACHM to determine whether therapy will be successful. Our study can offer specific guidelines for optimizing a pretherapeutic cortical imaging workup for the selection of suitable patients for therapy. Based on our study, we suggest the following recommendations for a minimal fMRI-based V1 mapping protocol in ACHM: (1) photopic testing ($\geq$7 cd/m^2) is preferable to scotopic testing. (2) Either conventional eccentricity or pRF mapping can be applied. (3) V1 boundaries can be determined by applying appropriate anatomic atlases[53,54] using a high-resolution anatomic scan. This results in a scanning session of approximately 30 min (15 minutes of anatomic/preparatory scans + 15 minutes of mapping scans). A similar workup could also be useful as an objective measure of the state of the visual cortex in other visual system disorders.[56,76–78] Similarly, previous fMRI investigations of early visual cortex have demonstrated the value of using anatomic atlases[53,54] to characterize anatomic and functional signatures in patient-related studies.[71,79,80] Further studies are needed to assess how these techniques can be used to identify objective biomarkers for therapy success, beyond their potential for a preclinical workup.

Limitations

Multicenter studies are advantageous, particularly for studying rare diseases, but they can also introduce potential limitations as not all scanner, stimulation, and analysis settings can be matched perfectly. While we intended to minimize site differences in the current study, several factors required flexibility for some settings. We addressed this with a specific cross-site statistical comparison of fMRI signal coherence. Importantly, this is a measure that is at the end of the acquisition/processing chain. Consequently, if there were relevant site effects, they should be expected to accumulate in this measure. At the same time, signal coherence is directly linked to the outcome measure and thus the result of the study. The presence of the physiologically expected luminance effect, independent of site, and the absence of site and interaction effects clearly indicate that site differences in stimulus luminance, scanner parameters, and data processing do not significantly affect the study outcome.

Another limitation is related to fixation instabilities. Persons with achromatopsia tend to have nystagmus, however of low amplitude and high frequency. The potential of nystagmus to reduce the validity of retinotopic mapping data in the context of visual system plasticity has previously been explicitly addressed via simulations in ACHM[31] and early blindness.[58] These authors demonstrated that nystagmus and fixation instability result in an enlargement of the pRF sizes, as reported in the present study for ACHM, while it does not have major effects on the actual eccentricity and polar angle mapping measures. Nystagmus in ACHM might therefore not be a relevant confound, as pRF sizes were not valued as an informative outcome measure in our study. Instead, we used a statistical design that reduces overall effects, such as nystagmus, on fMRI activation (i.e., as the critical measure in the analysis served the interaction of ROI with activated cortex or with eccentricity). This way, one ROI serves as an intraindividual reference reducing potentially confounding overall effects, such as nystagmus, on the cortical responses.

Conclusion and Outlook

We report a substantial deafferentation of the primary visual cortex in ACHM from retinal cone input. At the group level, cortical maps were found to be remarkably stable, suggesting limitations to the degree of plasticity of the foveal representation in the human primary visual cortex, even in congenital visual system abnormalities. As large-scale remapping of the foveal representation was not evident at the group level in ACHM, restoring retinal input to the visual cortex is not generally expected to result in sensory conflict that could result from remapping. This is encouraging news for those developing treatments for ACHM that aim to restore cone function at the retinal level. However, a detailed pretherapeutic workup to characterize cortical organization is advisable, especially during the exploratory phase of novel therapies.

Acknowledgments

The authors thank the German patient association "Achromatopsie Selbsthilfe e.V." for support in participant recruitment.

Supported by European Union's Horizon 2020 research and innovation program under the Marie Sklodowska-Curie grant agreement (No. 641805) and the German Research Foundation (DFG, HO 2002/12-1; 618139).

Disclosure: **B. Molz**, None; **A. Herbik**, None; **H.A. Baseler**, None; **P. de Best**, None; **N. Raz**, None; **A. Gouws**, None; **K. Ahmadi**, None; **R. Lowndes**, None; **R.J. McLean**, None; **I. Gottlob**, None; **S. Kohl**, None; **L. Choritz**, None; **J. Maguire**, None; **M. Kanowski**, None; **B. Käsmann-Kellner**, None; **I. Wieland**, None; **E. Banin**, None; **N. Levin**, None; **A.B. Morland**, None; **M.B. Hoffmann**, None

References

1. Ashtari M, Cyckowski LL, Monroe JF, et al. The human visual cortex responds to gene therapy–mediated recovery of retinal function. *J Clin Invest*. 2011;121:2160–2168.
2. Ashtari M, Zhang H, Cook PA, et al. Plasticity of the human visual system after retinal gene therapy in patients with Leber's congenital amaurosis. *Sci Transl Med*. 2015;7:296ra110.
3. Alexander JJ, Umino Y, Everhart D, et al. Restoration of cone vision in a mouse model of achromatopsia. *Nat Med*. 2007;13:685–687.
4. Banin E, Gootwine E, Obolensky A, et al. Gene augmentation therapy restores retinal function and visual behavior in a sheep model of CNGA3 achromatopsia. *Mol Ther*. 2015;23:1423–1433.
5. Carvalho LS, Xu J, Pearson RA, et al. Long-term and age-dependent restoration of visual function in a mouse model of CNGB3-associated achromatopsia following gene therapy. *Hum Mol Genet*. 2011;20:3161–3175.
6. Komáromy AM, Alexander JJ, Rowlan JS, et al. Gene therapy rescues cone function in congenital achromatopsia. *Hum Mol Genet*. 2010;19:2581–2593.
7. Michalakis S, Mühlfriedel R, Tanimoto N, et al. Restoration of cone vision in the CNGA3-/- mouse model of congenital complete lack of cone photoreceptor function. *Mol Ther*. 2010;18:2057–2063.

8. Pang JJ, Deng WT, Dai X, et al. AAV-mediated cone rescue in a naturally occurring mouse model of CNGA3-achromatopsia. *PLoS One*. 2012;7:e35250.
9. Farahbakhsh M, Anderson EJ, Maimon-Mor RO, et al. A demonstration of cone function plasticity after gene therapy in achromatopsia. *Brain*. 2022;145:3803–3815.
10. McKyton A, Averbukh E, Ohana DM, et al. Cortical visual mapping following ocular gene augmentation therapy for achromatopsia. *J Neurosci*. 2021;41:7363.
11. Reichel FF, Michalakis S, Wilhelm B, et al. Three-year results of phase I retinal gene therapy trial for CNGA3-mutated achromatopsia: results of a non randomised controlled trial. *Br J Ophthalmol*. 2021;106:1567–1572.
12. Fischer MD, Michalakis S, Wilhelm B, et al. Safety and vision outcomes of subretinal gene therapy targeting cone photoreceptors in achromatopsia: a nonrandomized controlled trial. *JAMA Ophthalmol*. 2020;138:643–651.
13. Aboshiha J, Dubis AM, Cowing J, et al. A prospective longitudinal study of retinal structure and function in achromatopsia. *Invest Ophthalmol Vis Sci*. 2014;55:5733–5743.
14. Michalakis S, Schön C, Becirovic E, Biel M. Gene therapy for achromatopsia. *J Gene Med*. 2017;19:e2944.
15. Zobor D, Zobor G, Kohl S. Achromatopsia: on the doorstep of a possible therapy. *Ophthalmic Res*. 2015;54:103–108.
16. Mühlfriedel R, Tanimoto N, Schön C, et al. AAV-mediated gene supplementation therapy in achromatopsia type 2: preclinical data on therapeutic time window and long-term effects. *Front Neurosci*. 2017;11:292.
17. Poloschek CM, Kohl S. Achromatopsie. *Ophthalmologe*. 2010;107:571–582.
18. Kohl S, Jägle H, Wissinger B, Zobor D. Achromatopsia. *GeneReviews*. 2018, https://www.ncbi.nlm.nih.gov/books/NBK1418/. Accessed May 5, 2022.
19. Solaki M, Baumann B, Reuter P, et al. Comprehensive variant spectrum of the CNGA3 gene in patients affected by achromatopsia. *Hum Mutat*. 2022:43:832–858.
20. Sun W, Li S, Xiao X, et al. Genotypes and phenotypes of genes associated with achromatopsia: a reference for clinical genetic testing. *Mol Vis*. 2020;26:588.
21. Haak KV, Cornelissen FW, Morland AB. Population receptive field dynamics in human visual cortex. *PLoS One*. 2012;7:1–8.
22. Haak KV, Morland AB, Engel SA. Plasticity, and its limits, in adult human primary visual cortex. *Multisens Res*. 2015;28:297–307.
23. Hoffmann MB, Dumoulin SO. Congenital visual pathway abnormalities: a window onto cortical stability and plasticity. *Trends Neurosci*. 2015;38:55–65.
24. Morland AB. Organization of the central visual pathways following field defects arising from congenital, inherited, and acquired eye disease. *Annu Rev Vis Sci*. 2015;1:329–350.
25. Wandell BA, Smirnakis SM. Plasticity and stability of visual field maps in adult primary visual cortex. *Nat Rev Neurosci*. 2009;10:873–884.
26. Prabhakaran GT, Al-Nosairy KO, Tempelmann C, et al. Functional dynamics of deafferented early visual cortex in glaucoma. *Front Neurosci*. 2021;15:653632.
27. Barton B, Brewer AA. fMRI of the rod scotoma elucidates cortical rod pathways and implications for lesion measurements. *Proc Natl Acad Sci*. 2015;112:5201–5206.
28. Prabhakaran GT, Carvalho J, Invernizzi A, et al. Foveal pRF properties in the visual cortex depend on the extent of stimulated visual field. *Neuroimage*. 2020;222:117250.
29. Baker CI, Dilks DD, Peli E, Kanwisher N. Reorganization of visual processing in macular degeneration: replication and clues about the role of foveal loss. *Vision Res*. 2008;48:1910–1919.
30. Baker CI, Peli E, Knouf N, et al. Reorganization of visual processing in macular degeneration. *J Neurosci*. 2005;25:614–618.
31. Baseler HA, Brewer AA, Sharpe LT, et al. Reorganization of human cortical maps caused by inherited photoreceptor abnormalities. *Nat Neurosci*. 2002;5:364–370.
32. Molz B, Herbik A, Baseler HA, et al. Structural changes to primary visual cortex in the congenital absence of cone input in achromatopsia. *Neuroimage Clin*. 2022;33:102925.
33. Lowndes R, Molz B, Warriner L, et al. Structural differences across multiple visual cortical regions in the absence of cone function in congenital achromatopsia. *Front Neurosci*. 2021;15:1331.
34. McCulloch DL, Marmor MF, Brigell MG, et al. ISCEV standard for full-field clinical electroretinography (2015 update). *Doc Ophthalmol*. 2015;130:1–12.
35. Brainard DH. The Psychophysics Toolbox. *Spat Vis*. 1997;10:433–436.
36. Kleiner M, Brainard DH, Pelli DG, et al. What's new in Psychtoolbox-3? A free cross-platform toolkit for psychophysiscs with Matlab and GNU/Octave. *Cogn Comput Psychophys*. 2007;36:1–89.
37. Pelli DG. The VideoToolbox software for visual psychophysics: transforming numbers into movies. *Spat Vis*. 1997;10:437–442.
38. Engel SA, Glover GH, Wandell BA. Retinotopic organization in human visual cortex and the spatial precision of functional MRI. *Cerebral Cortex*. 1997;7:181–192.
39. Engel SA, Rumelhart DE, Wandell BA, et al. FMRI of human visual cortex. *Nature*. 1994;369:525.
40. Wandell BA, Dumoulin SO, Brewer AA. Visual field maps in human cortex. *Neuron*. 2007;56:366–383.
41. Dumoulin SO, Wandell BA. Population receptive field estimates in human visual cortex. *Neuroimage*. 2008;39:647–660.
42. Clarke FJJ. A study of Troxler's effect. *Optica Acta*. 1960;7:219–236.
43. Crovitz HF, Zener K. A group-test for assessing hand- and eye-dominance. *Am J Psychol*. 1962;75:271–276.
44. Li J, Lam CSY, Yu M, et al. Quantifying sensory eye dominance in the normal visual system: a new technique and insights into variation across traditional tests. *Invest Opthalmol Vis Sci*. 2010;51:6875.
45. Kommerell G, Schmitt C, Kromeier M, Bach M. Ocular prevalence versus ocular dominance. *Vision Res*. 2003;43:1397–1403.
46. Fischl B, Sereno MI, Dale AM. Cortical surface-based analysis: II. Inflation, flattening, and a surface-based coordinate system. *Neuroimage*. 1999;9:195–207.
47. Somers DC, Dale AM, Seiffert AE, Tootell RBH. Functional MRI reveals spatially specific attentional modulation in human primary visual cortex. *Proc Natl Acad Sci USA*. 1999;96:1663–1668.
48. Yushkevich PA, Piven J, Hazlett HC, et al. User-guided 3D active contour segmentation of anatomical structures: significantly improved efficiency and reliability. *Neuroimage*. 2006;31:1116–1128.
49. Zhang Y, Brady M, Smith SM. Segmentation of brain MR images through a hidden Markov random field model and the expectation-maximization algorithm. *IEEE Trans Med Imaging*. 2001;20:45–57.
50. Jenkinson M, Bannister P, Brady M, Smith SM. Improved optimization for the robust and accurate linear registration and motion correction of brain images. *Neuroimage*. 2002;17:825–841.
51. Kaule FR, Wolynski B, Gottlob I, et al. Impact of chiasma opticum malformations on the organization of the human ventral visual cortex. *Hum Brain Mapp*. 2014;35:5093–5105.

Investigative Ophthalmology & Visual Science

52. Baseler HA, Gouws AD, Haak KV., et al. Large-scale remapping of visual cortex is absent in adult humans with macular degeneration. *Nat Neurosci*. 2011;14:649–657.
53. Benson NC, Butt OH, Brainard DH, Aguirre GK. Correction of distortion in flattened representations of the cortical surface allows prediction of V1-V3 functional organization from anatomy. *PLoS Comput Biol*. 2014;10:e1003538.
54. Benson NC, Winawer J. Bayesian analysis of retinotopic maps. *Elife*. 2018;7:e40224.
55. Vernon RJW, Gouws AD, Lawrence SJD, et al. Multivariate patterns in the human object-processing pathway reveal a shift from retinotopic to shape curvature representations in lateral occipital areas, LO-1 and LO-2. *J Neurosci*. 2016;36:5763–5774.
56. Ritter M, Hummer A, Ledolter AA, et al. Correspondence between retinotopic cortical mapping and conventional functional and morphological assessment of retinal disease. *Br J Ophthalmol*. 2019;103:208–215.
57. Silver MA, Ress D, Heeger DJ. Topographic maps of visual spatial attention in human parietal cortex. *J Neurophysiol*. 2005;94:1358–1371.
58. Levin N, Dumoulin SO, Winawer J, et al. Cortical maps and white matter tracts following long period of visual deprivation and retinal image restoration. *Neuron*. 2010;65:21–31.
59. Haak KV, Langers DRM, Renken R, et al. Abnormal visual field maps in human cortex: a mini-review and a case report. *Cortex*. 2014;56:14–25.
60. Ahmadi K, Herbik A, Wagner M, et al. Population receptive field and connectivity properties of the early visual cortex in human albinism. *Neuroimage*. 2019;202:116105.
61. Fracasso A, Petridou N, Dumoulin SO. Systematic variation of population receptive field properties across cortical depth in human visual cortex. *Neuroimage*. 2016;139:427–438.
62. Klein BP, Harvey BM, Dumoulin SO. Attraction of position preference by spatial attention throughout human visual cortex. *Neuron*. 2014;84:227–237.
63. Ahmadi K, Fracasso A, Puzniak RJ, et al. Triple visual hemifield maps in a case of optic chiasm hypoplasia. *Neuroimage*. 2020;215:116822.
64. Hoffmann MB, Tolhurst DJ, Moore AT, Morland AB. Organization of the visual cortex in human albinism. *J Neurosci*. 2003;23:8921–8930.
65. DeYoe EA, Ulmer JL, Mueller WM, et al. Imaging of the functional and dysfunctional visual system. *Semin Ultrasound CT MRI*. 2015;36:234–248.
66. Aguirre GK, Datta R, Benson NC, et al. Patterns of individual variation in visual pathway structure and function in the sighted and blind. *PLoS One*. 2016;11:e0164677.
67. Noppeney U, Friston KJ, Ashburner J, et al. Early visual deprivation induces structural plasticity in gray and white matter. *Curr Biol*. 2005;15:R488–R490.
68. Pan WJ, Wu G, Li CX, et al. Progressive atrophy in the optic pathway and visual cortex of early blind Chinese adults: a voxel-based morphometry magnetic resonance imaging study. *Neuroimage*. 2007;37:212–220.
69. Park HJ, Lee JD, Kim EY, et al. Morphological alterations in the congenital blind based on the analysis of cortical thickness and surface area. *Neuroimage*. 2009;47:98–106.
70. Ptito M, Schneider FCG, Paulson OB, Kupers R. Alterations of the visual pathways in congenital blindness. *Exp Brain Res*. 2008;187:41–49.
71. Aguirre GK, Butt OH, Datta R, et al. Postretinal structure and function in severe congenital photoreceptor blindness caused by mutations in the GUCY2D gene. *Invest Ophthalmol Vis Sci*. 2017;58:959–973.
72. Bourgeois JP, Jastreboff PJ, Rakic P. Synaptogenesis in visual cortex of normal and preterm monkeys: evidence for intrinsic regulation of synaptic overproduction. *Proc Natl Acad Sci*. 1989;86:4297–4301.
73. Guerreiro MJS, Erfort MV, Henssler J, et al. Increased visual cortical thickness in sight-recovery individuals. *Hum Brain Mapp*. 2015;36:5265–5274.
74. Stryker MP, Harris WA. Binocular impulse blockade prevents the formation of ocular dominance columns in cat visual cortex. *J Neurosci*. 1986;6:2117–2133.
75. Glasser MF, van Essen DC. Mapping human cortical areas in vivo based on myelin content as revealed by T1- and T2-weighted MRI. *J Neurosci*. 2011;31:11597–11616.
76. Papanikolaou A, Keliris GA, Papageorgiou TD, et al. Population receptive field analysis of the primary visual cortex complements perimetry in patients with homonymous visual field defects. *Proc Natl Acad Sci*. 2014;111:E1656–E1665.
77. Silson EH, Aleman TS, Willett A, et al. Comparing clinical perimetry and population receptive field measures in patients with choroideremia. *Invest Ophthalmol Vis Sci*. 2018;59:3249–3258.
78. Smirnakis SM. Probing human visual deficits with functional magnetic resonance imaging. *Annu Rev Vis Sci*. 2016;2:171–195.
79. Cideciyan AV, Aleman TS, Boye SL, et al. Human gene therapy for RPE65 isomerase deficiency activates the retinoid cycle of vision but with slow rod kinetics. *Proc Natl Acad Sci*. 2008;105:15112–15117.
80. Winawer J, Parvizi J. Linking electrical stimulation of human primary visual cortex, size of affected cortical area, neuronal responses, and subjective experience. *Neuron*. 2016;92:1213–1219.

Investigative Ophthalmology & Visual Science